physica status solidi b
www.pss-b.com

Battery Powder as a Source of Novel Graphene Nanocarbons

Agnieszka Dąbrowska, Weronika Urbańska, Magdalena Warczak, and Magdalena Osial**

Lithium-ion batteries (LIBs) waste is classified as a dangerous one. Fortunately, LIBs can be recycled and are already a valuable source of metals. This work is focused on the properties of the spent LIBs powder, which is a postproduct of the proposed organic leaching process and is presented as a source of nanocarbons with a unique structure. Furthermore, attention is paid to revealing the properties of the carbon component that can find a second life in other applications like photocatalysis or sorbents. Raman spectroscopy is used for the characterization of graphitic carbon. Scanning electron microscopy images are numerically quantitatively analyzed to provide additional parameters (for instance, the total length of edges) about the structure of materials, and X-ray diffraction (XRD) and energy-dispersive X-ray spectroscopy (EDS) further check their composition.

1. Introduction

Since their commercialization in the 1990s, lithium-ion batteries (LIBs) have become an integral part of our life.[1] The increase in the popularity of portable electronics such as smartphones, laptops, and others contributed to the dynamic growth in battery production. Furthermore, the application of LIBs in electric cars in 2010 boosted the enormous development of LIBs that we see now.[2] LIBs are currently one of the most commonly used energy sources for portable electronics like laptops, mobile phones, and even electric vehicles. They are also gradually replacing less technologically advanced nickel–metal hydride (Ni–MH) accumulators, mainly in the global automotive industry. Statistical data on the management of portable batteries in the European Union member states confirm these assumptions and indicate a dynamic increase in the mass of cells introduced to the market in 2010–2018.[3–6] Forecasts for the development of technologies used in the production of portable batteries and accumulators and quantitative data from eight reporting years in the EU countries indicate that this trend will be maintained in the coming years.

The growing number of manufactured and more willingly used batteries, including Li-ion cells, significantly increases the amount of their waste. In Poland, as there are no precise reports on the mass of collected waste LIBs or even their collection levels, certain assumptions should be made to estimate the current waste Li-ion cell stream's current mass and forecast. For the calculations, it was assumed that: 1) LIBs constitute 80% of batteries introduced to the market included in the group "other;"[7–10] 2) the annual growth of LIBs introduced into the market is equal to the average growth of these batteries in 2010–2018 and amounts to 5%; and 3) the collection rate of spent LIBs is equal to the annual minimum required level of collection of all types of portable waste batteries in a given year.[11]

The performed forecast of the mass of collected waste LIBs by 2030 is shown in **Figure 1**.

The forecasts indicate that in 2021 in Poland alone, the mass of spent LIBs may be over 1600 tons, while in 2030, there will be about 1000 tons more. This trend is also present in foreign data. In the publication of the European Commission on cost scenarios and growth of the LIB market, it was stated that the growing popularity of electric vehicles (EVs) had the most significant impact on the increase in the number of produced batteries of this type.[12] It is assumed that in 2028 50–200 million EVs will be used, and in 2040, even 900 million. Therefore, the demand for Li-ion accumulators will increase from 77 GWh (2018) to 600–4000 GWh (2040). In addition, it is estimated that the global LIB market will be worth 200 billion euros by 2040, which will also significantly contribute to the increase in the amount of their waste in the coming years.

Due to their properties and various chemical substances, spent LIBs are often classified as hazardous waste–posing a

A. Dąbrowska, M. Osial
Faculty of Chemistry
University of Warsaw
Pasteura 1, 02-093 Warsaw, Poland
E-mail: adabrowska@chem.uw.edu.pl; mosial@chem.uw.edu.pl

A. Dąbrowska
Biological and Chemical Research Centre
University of Warsaw
Żwirki i Wigury 101, 02-089 Warsaw, Poland

W. Urbańska
Faculty of Environmental Engineering
Wrocław University of Science and Technology
Wybrzeże Wyspiańskiego 27, 50-370 Wrocław, Poland

M. Warczak
Institute of Physical Chemistry
Polish Academy of Sciences
Kasprzaka 44/52 Street, 01-224 Warsaw, Poland

M. Osial
Department of Theory of Continuous Media and Nanostructures
Institute of the Fundamental Technological Research
Polish Academy of Sciences
Adolfa Pawińskiego 5B, 02-106 Warsaw, Poland

The ORCID identification number(s) for the author(s) of this article can be found under https://doi.org/10.1002/pssb.202100588.

DOI: 10.1002/pssb.202100588

 © 2022 Wiley-VCH GmbH

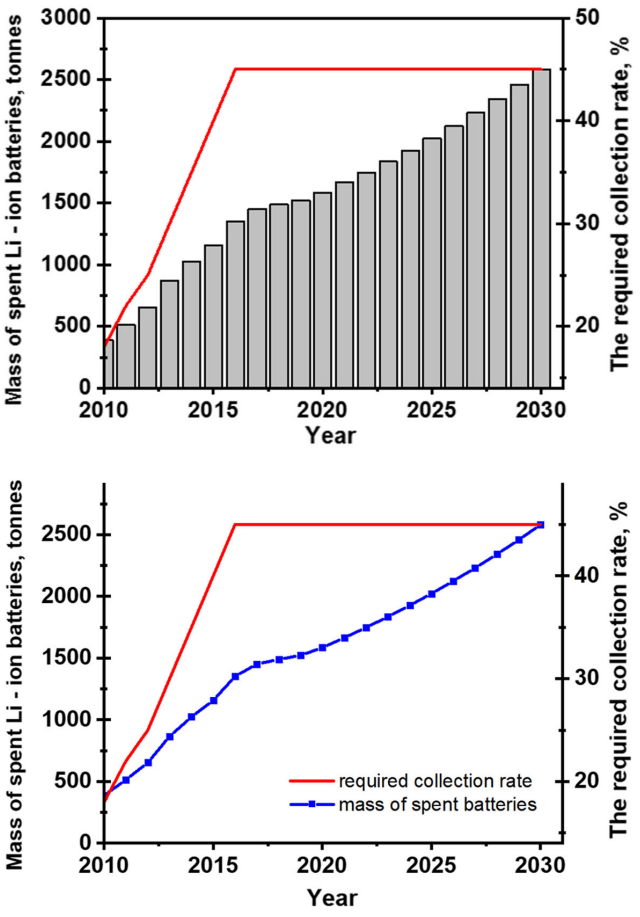

Figure 1. Mass of collected waste LIBs in Poland—forecast until 2030—histogram; the required collection rate is presented as a red curve on the graph.

threat to the natural environment and human health requiring appropriate treatment. Otherwise, heavy metals and the other components of LIBs can have a dramatic effect on health.[13–15]

The chemical composition of the different LIBs varies primarily with the chemicals used to form the electrolyte and electrodes, especially the cathode material. The most commonly used types of LIBs include LCO (cathode—$LiCoO_2$), LMO (cathode—$LiMn_2O4_4$), NMC (cathode—$LiNiMnCoO_2$), LFP (cathode—$LiFePO_4$), and NCA (cathode—$LiNiCoAlO_2$).[16] The most popular cells used by users of electronic equipment are LCO batteries with a cathode in the form of $LiCoO_2$. The batteries also consist of other materials, including plastic or steel.[17]

Besides these metals, spent battery waste is a tremendous source of graphitic carbon that is one of the top listed materials for electrocatalytic use, mainly because different types of carbon-based materials are employed as anodes in LIBs. It is all due to the considerable large surface area needed for high capacity and light devices, high conductivity and fast-charge/discharge devices, and extensive mechanical and chemical resistance.[18] Therefore, there are attempts to recover carbon materials[19] from LIBs waste, especially graphene,[20] which is a highly desired material due to its unique physical and chemical properties. Depending on the recycling method, graphite can be recovered directly from battery waste using, e.g., hydrometallurgical route or indirectly by further modification of recovered material. For instance, nanocomposite films based on reduced graphene oxide (rGO) can be obtained using Hummer's method and a chemical reduction.[21]

Spent lithium battery waste became a severe environmental problem. They contain many toxic substances, for example, heavy metals like Co, Cr, Mo, Ni, and Mn, and different organic electrolytes.[22–24] Still, many of the waste LIBs land in the environment leading to the inevitable contamination of the soil, ground and underground water, and the air. At the same time, they became a valuable source of various materials. Therefore, their proper recovery and reuse are essential for environmental protection and health.[25–27] Many precious metals are removed or partially recycled from the spent LIBs powder within the leaching process, while the carbon-based core still does not have economic applications. In this work, the main emphasis is made to present the potential of the use of postleaching waste LIBs powder as a promising source of carbon.

Within this study, LIBs were proved to be a source of valuable nanocarbons materials whose presence was confirmed by Raman spectroscopy and morphological analyses. Furthermore, the battery waste was treated with acid leaching, which recently brought lots of attention for its processing, economic and environmental aspects, high purity postproducts, high selectivity, recovery rate, and low energy consumption.[28–31]

2. Experimental Section

2.1. Battery Powders Treatment

In this work, the stream of LIBs' types was undergoing the acid leaching procedure to recover the different metals. Spent batteries were obtained from numerous sources of spent electronic waste, and the mainstream LIBs mainly contained the cells from Hewlett–Packard, Lenovo, or Toshiba. Initially, the batteries were treated manually, where the main components were defragmented to separate metals from the plastics. Then, the anode and the cathode were separated within the procedure described previously.[32] Finally, the electrodes were treated with acid and reducing agents. While in this work, formic acid was proposed as a bleaching agent, and glutaric acid and hydrogen peroxide was used as reducing agents.

2.2. Chemical Purification

The first step after the mechanical separation of the waste battery components was the mineralization process, where the 0.5 g of waste battery powder containing both cathode and anode was treated with 10.0 mL of the 65% HNO_3 (analytical grade, purchased from POCH, Poland) for about 5 h and the temperature of about 120 °C. Then, the obtained solution was evaporated to approximately 0.5 mL, transferred quantitatively to a plastic container, and supplemented with deionized water to 50 g. Finally, the metal concentrations in the solution were determined using inductively coupled plasma optical emission spectrometry (ICP-OES), Agilent 720.

Second, the obtained powder was treated with the following agents: sample 1 was treated with 5.0 M formic acid CH_2O_2

© 2022 Wiley-VCH GmbH

Table 1. Leaching agents for samples 1–3.

Sample 1	Sample 2	Sample 3
5.0 M formic acid CH_2O_2	5.0 M formic acid CH_2O_2 + 0.9% v/v hydrogen peroxide H_2O_2	5.0 M formic acid CH_2O_2 + 0.9% v/v hydrogen peroxide H_2O_2 + 5 g glutaric acid $C_5H_8O_4$

(85% analytical grade, Chempur), sample 2 was leached with 5.0 M formic acid and hydrogen peroxide H_2O_2 (30% analytical grade, STANLAB; 0.9% v/v), and sample 3 was treated with both formic acid and hydrogen peroxide, while, additionally, the 5 g of glutaric acid $C_5H_8O_4$ powder was added (5% analytical grade, STANLAB) (see **Table 1**). Organic acids and H_2O_2 worked as reducing agents for metals recovery in acidic media.[33,34]

In our previous work, the waste battery powder was heated to a milder temperature of about 90 °C and a time of about 2 h, where the residue was continuously stirred at the rate of about 500 rpm. After the treatment, the waste battery powders were washed with deionized water to remove leaching agents and dried without a protective atmosphere at 50 °C under the fume hood. **Figure 2** shows the schematic diagram of the battery powder leaching process for sample 3.

2.3. Raman Spectroscopy

The Raman spectra were collected on DXR Raman Microscope (Thermo Scientific) with the three laser lines: 455, 532, and 633 nm. The standard green laser line (532 nm) chosen from the four available (including 455, 633, and 780 nm) was used for the quantitative characterization and compared with other data sets. The exposure time was set to 50 s, 50 repetitions (20 in subsequent control measurements). The aperture was 50 mm, and the power of the laser beam was 10 mW. Each sample was measured at least several dozen times (from 80 to >300) in different places. The average signal had the background cut off according to the four algorithms described in Section 2.4. Representative Raman spectra for all samples are given in Figure S1, Supporting Information. Four spectra were collected for samples 1 and 3 (Figure S2 and S3, Supporting Information, respectively). Six varying spectra were registered for sample 3 (Figure S3, Supporting Information).

2.4. Numerical Analyses

For the numerical analysis, the following software were used: OMNIC (together with the libraries), ORIGIN, and Python scripts (signal deconvolution, peak search, and calculation of a surface area of G and D peaks). Four types of baselines were tested to cut off the background:

@_ OMNIC standard,

A_ Adaptive iteratively reweighted penalized least squares AIRPLS as described and coded in ref. [35],

B_ Asymmetrically reweighted penalized least squares ARPLS,[36]

C_ Asymmetric Least Squares Smoothing ALSS as in ref. [37]. One can find the upgrade of this approach in ref. [38].

2.5. Characterization of Samples

The content of metal ions in the solutions was investigated with ICP-OES—Agilent 720. The morphology was studied with scanning electron microscopy (SEM). The microscope Merlin (Zeiss) equipped with a Gemini II column was used. The device worked in the low kV value range (0.5–1.5 kV) and low probe current of 10–20 μA. Kα lines obtained by the energy-dispersive X-ray spectroscopy (EDS) were used for elemental analysis of the measured samples with the 15 kV accelerating voltage, 6 mm working distance, and 5 min for a single map collection under the vacuum conditions of about 2×10^{-5} Torr. The powder X-ray diffraction patterns were recorded with a powder diffraction X-ray diffractometer (PXRD) X'PERT Phillips with PW 1830 generator with Cu Kα radiation with line $\lambda = 1.5405980$ Å and a scan rate of 1° min^{-1} in 0.016° steps covering the 2θ angle range from 18° to 85°. The thermal stability of the postleached waste battery powder was evaluated by thermogravimetric (TGA) using a TG 209 F3 Tarsus apparatus (Netzsch). The samples were heated at a rate of 10 °C min^{-1} in an ambient nitrogen atmosphere, 30–900 °C.

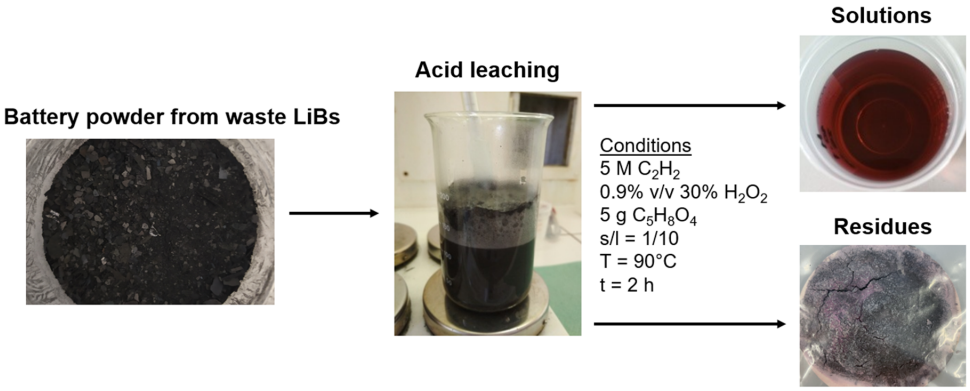

Figure 2. Schematic diagram of the leaching procedure to obtain the residue for sample 3.

© 2022 Wiley-VCH GmbH

3. Results and Discussion

3.1. Qualitative Analysis

The solution obtained from the leaching procedure was investigated with ICP-OES to indicate the number of particular elements to be successfully leached. **Figure 3** presents the recovery rate of seven metals found in the postleaching solutions.

Depending on the experimental conditions applied to the waste LIBs powder, the recovery of the particular metals was different. Therefore, the obtained results of metal recovery are presented as percentage rates, calculated in relation to the content of ions of the tested metals in the battery powder before chemical treatment. The rates were calculated according to Equation (1)

$$\text{Recovery rate}\,[\%] = \frac{\text{Me}_{\text{ls}}\left[\frac{\text{mg}}{\text{kg}}\right]}{\text{Me}_{\text{in}}\left[\frac{\text{mg}}{\text{kg}}\right]} \times 100\% \quad (1)$$

where Me_{in} is concentration of test metal ions in the battery powder before leaching [mg kg^{-1}]; Me_{ls} is concentration of test metal ions in the solution after leaching [mg kg^{-1}].

The presentation of the battery powder leaching results in the percentage recovery rates of the tested metals, allows the best expression of metal recovery efficiency, and facilitates an interpretation of the outcomes.

For sample 1, the highest recovery was observed for Cu, Fe, and Zn, while the Co and Cr recovery was lower from a carbon-based matrix (Figure 3). Despite not fully recovered metals from the battery waste, the application of formic acid gave satisfactory results. In comparison to the literature procedures, the proposed procedure does not need to apply sulfuric acid to leach metals. Next, sample 2 was leached at the same formic acid content, while additionally hydrogen peroxide was used as a reducing agent. However, the recovery of metals is much lower than in

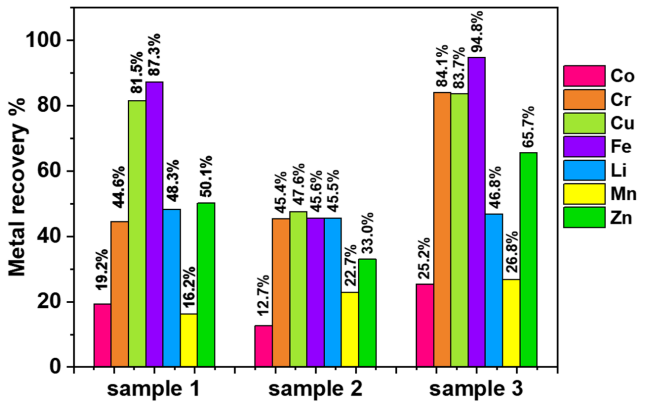

Figure 3. Degrees of metal recovery from solutions after acidic reductive leaching.

Table 2. Average values for samples 1–3. RBS—Raman band separation factor.

Parameter	Sample 1	Sample 2	Sample 3
G/D ratio (all baselines)	4.5	3.6	8.7
RBS (range)	220–231	228–247	216–249
G/D ratio (only OMNIC baseline)	7.14	4.50	9.66
RBS (only OMNIC baseline)	226.35	232.68	229.97
RBS (deconvoluted peaks)	230	229	222

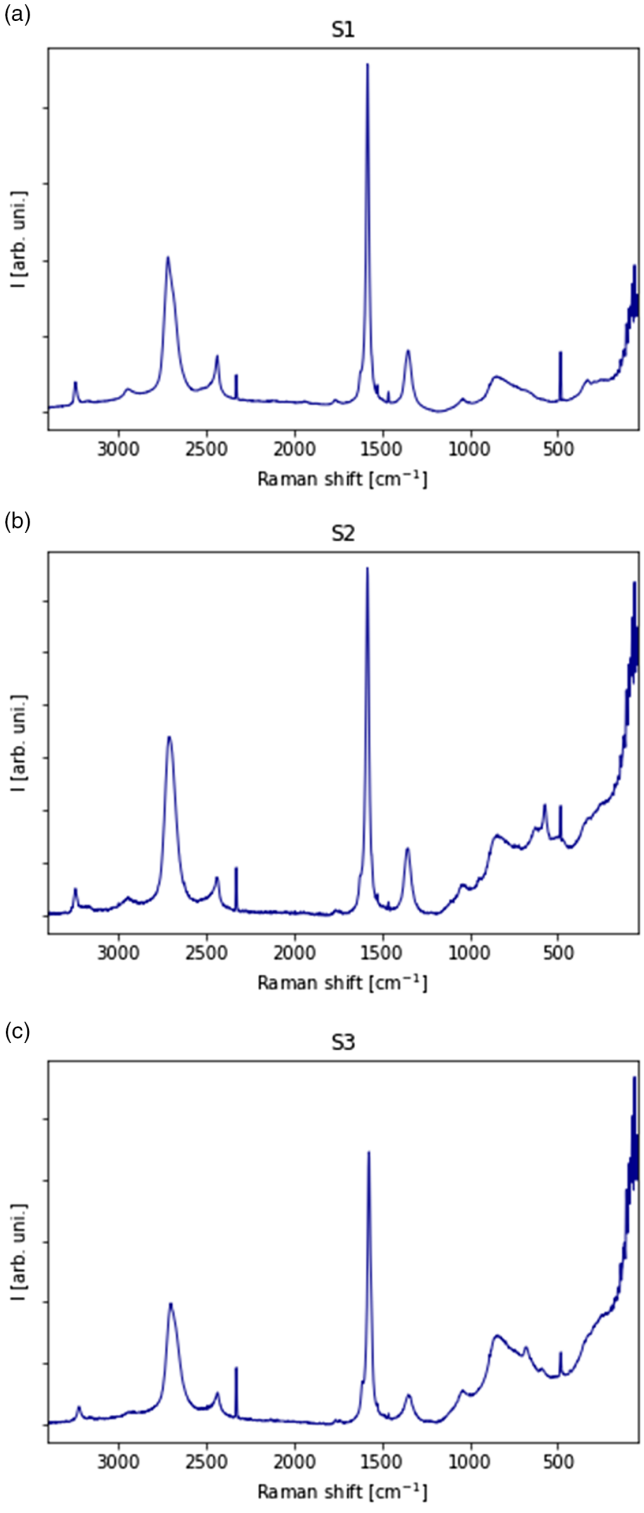

Figure 4. Raman spectra of samples: a) 1, b) 2, and c) 3.

© 2022 Wiley-VCH GmbH

sample 1. Primarily, for Cu and Fe, the rate decreased by 50%. The procedure was modified to get higher metal recovery, where the glutaric acid was added. Surprisingly, the addition of another organic acid improved the recovery efficiency. Using both reducing agents made it possible to recover the highest content of Co, Cr, Cu, Fe, Li, Mo, and even Zn.

Based on these investigations, it is seen that the main component of the tested battery powder that was not leached contains all the found metals, mostly cobalt, lithium, and nickel.

What is more important than the partial recovery of the metals is the content of the carbon-based materials, presented within the following characterization. The leaching can be improved by changing the experimental conditions, like adding some other reductions or longer leaching time, while still the residue contains mainly graphitic carbon presented within the following studies.

3.2. Raman Spectroscopy of Nanocarbons

After the statistical validation of measurements, qualitative and quantitative analyses and comparison of materials (samples 1–3) were possible. Figure S1, Supporting Information, summarizes the spectra obtained for samples and the range of noted changes, and Figure S2, Supporting Information, presents used baselines.

Bands D, G, and 2D (≈1350, ≈1580, and ≈2680 cm^{-1}, respectively) were considered for the quantitative analyses. The Raman spectral signal can be used to determine the number of layers,[39] uniaxial strain,[40] the number of carriers and defects or surface configuration in graphene-like materials,[41] and it is a common approach in their characterization (with peaks intensities, half-widths, areas, Raman shifts considered).[42–52] The main drawbacks of the quantitative description of carbon powders are related to the profound internal changes in parameters. Thus, proper statistical analysis is needed, and mapping should be used instead of point measurements. The increasing G/D ratio indicates better structural ordering, fewer defects, and the presence of a 2D band is directly related to the number of graphitic layers. Raman band separation (RBS) factor is obtained by the difference in positions of D and G bands. Band 2D moves toward the higher Raman shift (Rs) values with increasing strain and the lower Rs for the changes due to the elongation and stretching.[41] The width of the G band indicates the number of the carrier in material and is the highest for large Rs and narrow peaks.

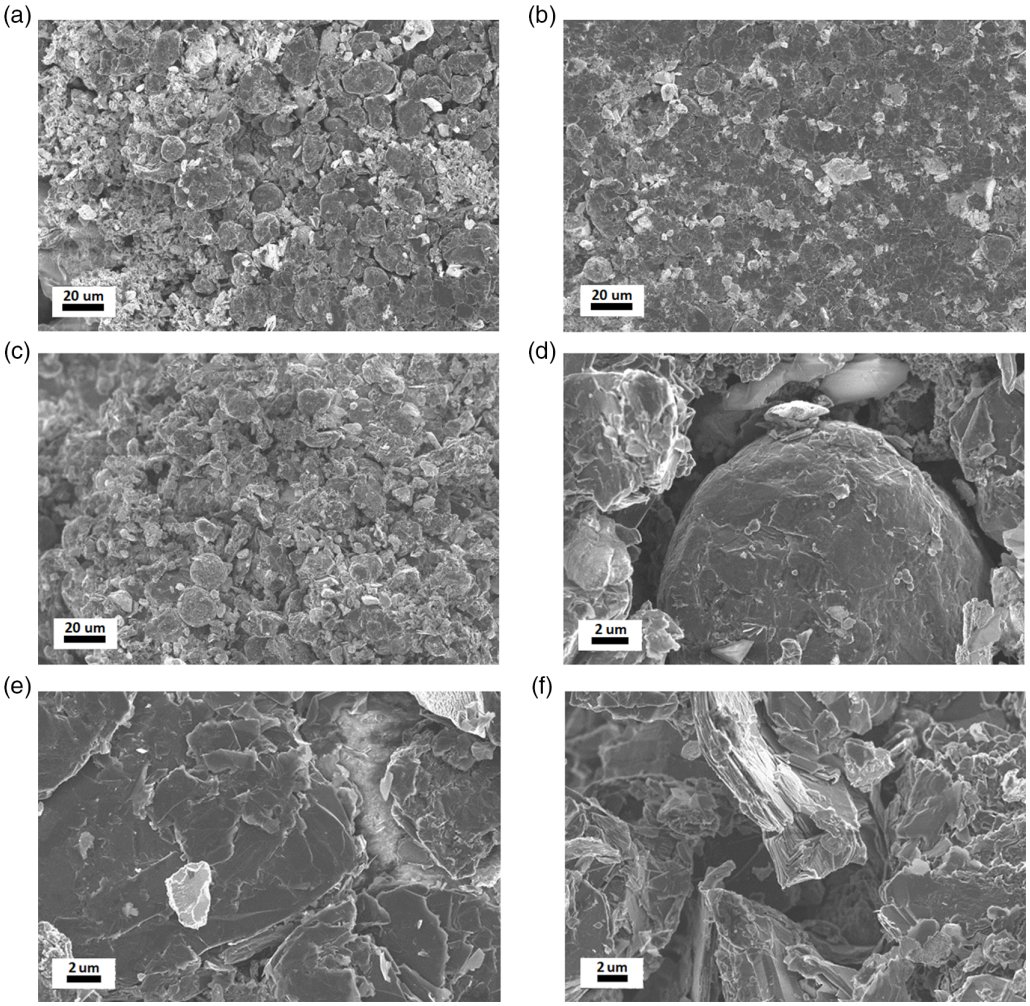

Figure 5. Lower and higher magnification of a,d) sample 1, b,e) sample 2, and c,f) sample 3.

© 2022 Wiley-VCH GmbH

Moreover, the G band can be separated into G+ and G− with increased mechanical strain. Band D was attributed to defects. Bands ≈360 and ≈1620 cm^{-1} typical for disordered carbons are absent. A reference graphite material would have:[41] 1) ≈1582 cm^{-1} (the so-called reference 0 band) owning to the E_{2g2} vibrational mode; ≈42 cm^{-1} for E_{2g1}; a sharp (10–15 cm^{-1}) graphitic band is usually present ≈1574–1580 cm^{-1}; 2) ≈2695 and ≈2735 cm^{-1} doublet for G'_1 and G'_2; and 3) ≈2440 and ≈3250 cm^{-1} weak bands.

The presence of a signal in these regions can be attributed to the traces of graphitic carbons. That is visible in all samples together with the different nanocarbons of the diverse structures. However, on average, the defects increase in the following order S3 < S1 < S2. Sample S2 exhibited many graphene-like flakes, but at the same time, metal oxide components and defects are also presented. The most homogenous is sample 3. Sample 1 has locally well-structured grains. The average results of quantitative analyses are collected in **Table 2**. Representative Raman spectra are collected in **Figure 4**. The intense and narrow G peak confirms the high quality of materials.[41]

The differences in morphology and the presence of heteroatoms convolute with the primary carbon signal. That is also visible within the Gauss peaks deconvolution.

3.3. Morphological Analyses

The morphology of the postleaching products was investigated with SEM (Merlin Zeiss). EDS was used for elemental analysis of the measured samples. All samples revealed graphene-like structures. The materials that build the electrodes, both cathode and anode, in LIBs are mainly made of graphitic carbon filled with electrolytes. As shown in **Figure 5**, the morphology of the following samples resembles grains having different shapes and sizes, while each of them is made of a flake-like structure. Each postleaching sample is similar in morphology on the macroscale, while in microscale (SEM) they differ considerably. It is due to the flake-like structure that can serve as a reused matrix for other compounds. Graphitic powder forms sphere-like structures that were further described in numerical analyses.

3.4. Numerical Characterization of Materials

SEM images were numerically analyzed to obtain a quantitative surface characterization. For instance, one can examine the shape of histograms to determine the homogeneity of a sample. The more diversified grain size distribution leads to a broader histogram. In contrast, the homogenous material with equal diameters presents a narrow band (**Figure 6**). The average grain sizes for debris in materials were estimated to be ≈60, ≈90, and ≈40 nm in samples 1–3, respectively.

Moreover, the total length of edges (Figure S3, Supporting Information) for a determined surface will directly indicate the surface properties and volume ratio. That is crucial, especially for sorbents. Therefore, values were obtained numerically by picture analysis of the corresponding SEM data. For example, the edges marked in samples 1–3 and their total length for 1 μm^2 were the following: 464.63, 292.52, and 333.53 nm.

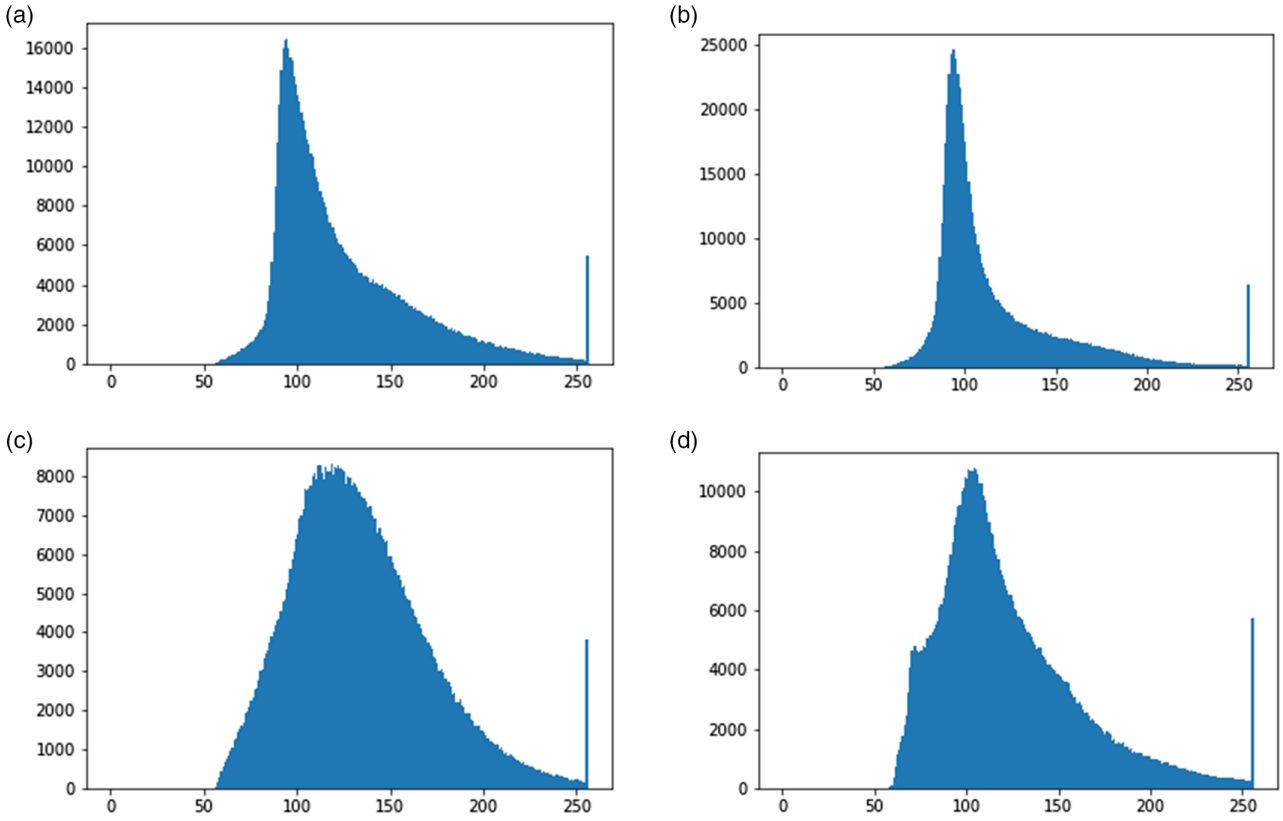

Figure 6. The histograms for a,b) sample 2 reveal a much more homogeneous structure (in both magnifications) than in c,d) sample 3.

© 2022 Wiley-VCH GmbH

Finally, the 3D reconstruction of morphology is possible from SEM pictures providing equal exposition (Figure S4, Supporting Information). It enables better visualization of the structure of a material.

Complementary, the EDS analysis was performed. Battery waste powder has the potential for further application as a catalytic material, especially for high carbon content and some traces of cobalt in samples. The highest carbon content in the sample is observed for sample 2. EDS elemental analysis confirmed the high efficiency of proposed leaching toward heavy metal removal.

Additionally, the elemental maps showing the distribution of the particular elements in the sample are presented in **Figure 7**, where the columns a–c correspond to samples 1–3, respectively. The colours shown in the figures are ascribed to carbon—red, cobalt—green, oxygen—blue, and manganese—yellow. The oxygen present in the sample mainly correlates with the cobalt, suggesting that the cobalt oxides in the sample can be a postproduct of the $LiCoO_2$ leaching.

3.5. Crystalographic Analysis

Due to the presence of some elements in the sample indicated by the EDS, the XRD analysis was also performed. The diffractogram presented in **Figure 8**a shows the patterns for samples 1–3. The chemical composition of all samples 1–3 shows presence of cobalt oxide traces. The powder patterns match to $LiCoO_2$ (reference material JCPDS 75-0532) and Co_3O_4 (reference material JCPDS 43-1003). The peak at about 19° visible in sample 3 can be ascribed to the $LiCoO_2$ (003), while the peaks at about 37° and 45° can be ascribed to the $LiCoO_2$ in (101) and (104).[53] Also, these peaks may be indexed as Co_3O_4 presence in the (111), (311), and (400) planes.[54] The characteristic, most intensive peak at about 27° can be attributed to the carbon in the (002) in all samples (as in the reference JCPDS 75-2078). Peaks at about 50° and 55° relate to the carbon in the graphitic form in the (102) and (104). The peak in the sample at about 77° and the following peak at about 84.2° also indicate the carbon in

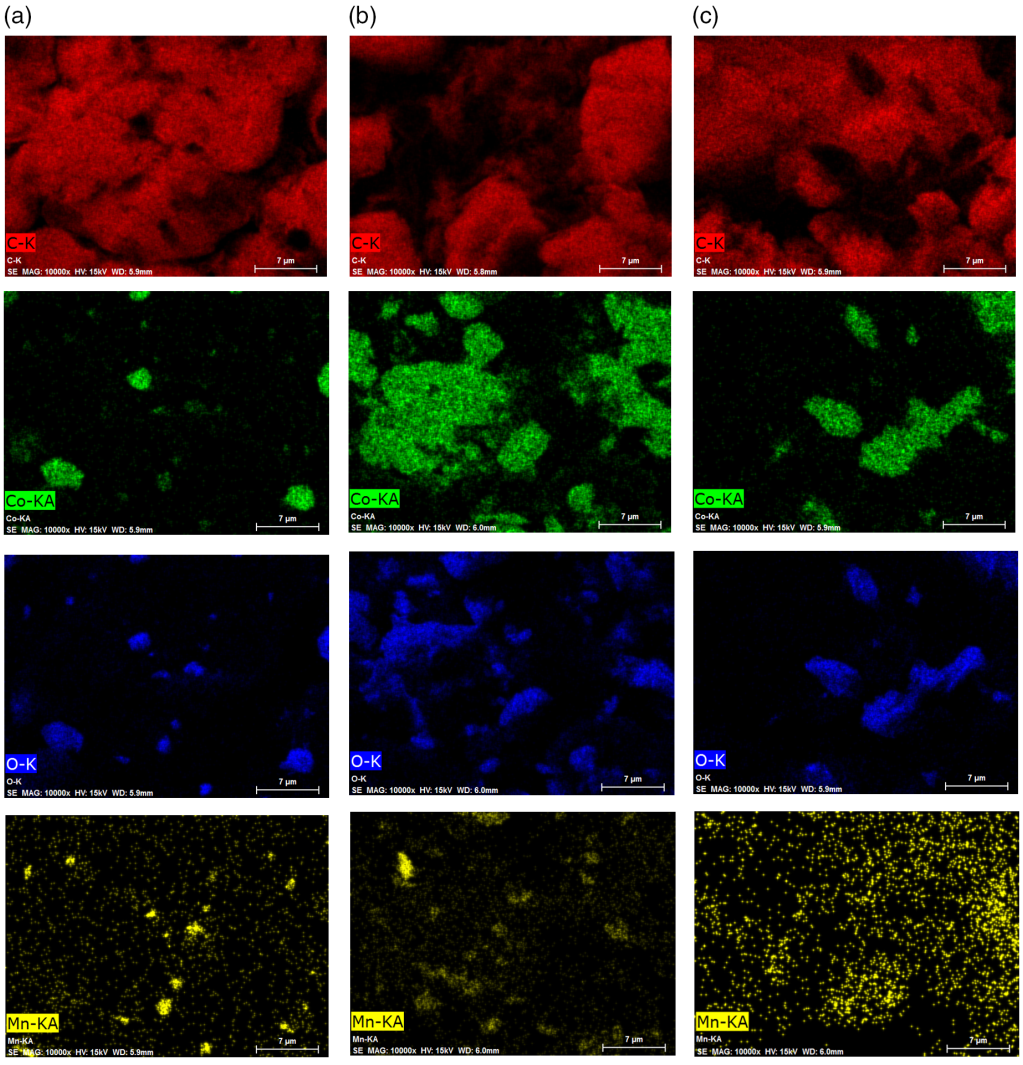

Figure 7. EDS maps for a) sample 1, b) sample 2, and c) sample 3, where the red corresponds to carbon, green to cobalt, oxygen is marked in blue, and manganese in yellow.

© 2022 Wiley-VCH GmbH

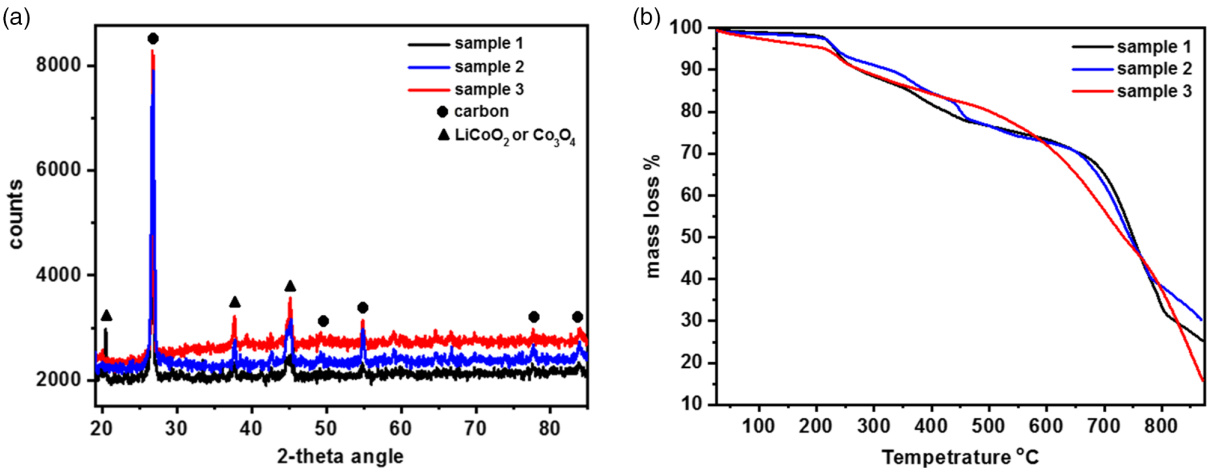

Figure 8. a) XRD patterns and b) TGA curves for samples 1–3.

(110) and (112) planes.[55,56] Data are in good agreement with the literature revealing that the postleaching product mainly contains the carbon product, namely, graphite, and some small traces of cobalt oxide,[57] while it is not excluded that the cobalt oxide can be partially present in the other form like manganese doped.[58] The manganese in the samples is in trace amounts, where the XRD does not point out characteristic manganese oxide patterns, so only some cobalt oxides can be identified.

The thermogravimetric measurements (TGA) were also performed in the nitrogen atmosphere. As shown in Figure 8b, the highest mass loss, corresponding to the oxidation of the carbon, is observed for sample 3. Lower mass loss for samples 1 and 2 can correlate with the higher metal oxides content in the samples.

4. Conclusions and Future Perspectives

Due to the growing pollution with battery waste, especially the carbon-based powder containing heavy metals, there is a tremendous need for their recovery and reuse. The problem will not disappear spontaneously, but large amounts of the spent battery, especially after the acid leaching, are promising for catalytic application, especially for significant carbon content and specific metals oxides. To do so, a deep analysis of postleaching products is needed. Although all tested materials were valuable sources of nanocarbons, they exhibited differences in morphology and structure ordering. Raman spectra reveal that all samples contain different nanocarbons in graphene-like and graphitic forms. The traces of other compounds are the most visible in sample 2. Additional EDS and XRD analysis also confirmed the presence of some cobalt oxides or lithiated cobalt oxide, while the postleaching product in the Co_3O_4 form is more probable to be formed in the sample. XRD data for sample 3 indicate that $LiCoO_2$ is the domiant Co phase. Based on the intensities of peaks, Co_3O_4 is dominant in samples 1, 2. Based on the XRD measurement, it was also possible to distinguish peaks characteristic of the samples' graphitic carbon. The proper background treatment is crucial for any numerical quantitative analysis within the Raman spectroscopy. All approaches confirmed highly structured carbons (S3 > S1 > S2), and the surface of flakes in powder favours their applications as sorbents. Overall, spent batteries can be a source of promising graphene-like nanomaterials for catalysis. That would be one of the future perspectives for this research.

Supporting Information

Supporting Information is available from the Wiley Online Library or from the author.

Acknowledgements

The authors are grateful to the following people and institutions: M.O. would like to thank UOTT UW for support with grant-funded under the Innovation Incubator 4.0 co-financed by Smart Growth Operational Programme 2014-2020; M.O. would like to thank Prof. Paweł Krysiński from the Faculty of Chemistry, the University of Warsaw, for hosting her in his laboratory; M.O. would also like to thank Prof. Michael Giersig from the Institute of the Fundamental Technological Research, Polish Academy of Sciences, for hosting her in his laboratory. A.D. is grateful to Prof. Barbara Pałys for the access to Raman spectroscopy, and Piotr Machowski for the substantial help in the programming and design of Python scripts. All authors would like to thank Katarzyna Skórczewska and Sławomir Wilczewski for TGA support.

Conflict of Interest

The authors declare no conflict of interest.

Data Availability Statement

The data that support the findings of this study are available in the supplementary material of this article.

Keywords

graphene materials, nanocarbons, organic acid leaching, Raman spectroscopy, spent Li-ion battery powder

© 2022 Wiley-VCH GmbH

Received: November 15, 2021
Revised: May 5, 2022
Published online:

[1] M. Winter, B. Barnett, K. Xu, *Chem. Rev.* **2018**, *118*, 11433.
[2] B. Diouf, R. Pode, *Renewable Energy* **2015**, *76*, 375.
[3] M. Pagliaro, F. Meneguzzo, *Heliyon* **2019**, *5* e01866.
[4] A. Sobianowska-Turek, *Waste Manage.* **2018**, *77*, 213.
[5] Z. Dobrowolski, Ł. Sułkowski, W. Danielak, *Energies* **2021**, *14*, 6273.
[6] J. Heelan, E. Gratz, Z. Zheng, Q. Wang, M. Chen, D. Apelian, Y. Wang, *JOM* **2016**, *68*, 2632.
[7] Z. Rogulski, A. Czerwiński, *J. Power Sources* **2006**, *159*, 454.
[8] E. Rudnik, J. Knapczyk-Korczak, *Metall. Res. Technol.* **2019**, *116*, 603.
[9] K. Krupa, Ł. Nieradko, A. Haraziński, *Energy Policy J.* **2018**, *21*, 19.
[10] K. Markowska, J. Flizikowski, K. Bieliński, A. Tomporowski, W. Kruszelnicka, R. Kasner, P. Bałdowska-Witos, Ł. Mazur, *Materials* **2021**, *14*, 4556.
[11] A. Sobianowska-Turek, W. Urbańska, *Batteries* **2019**, *5*, 72.
[12] I. Tsiropoulos, D. Tarvydas, N. Lebedeva, *Li-Ion Batteries for Mobility and Stationary Storage Applications – Scenarios for Costs and Market Growth*, Publications Office of the European Union, Luxembourg **2018**, https://doi.org/10.2760/87175.
[13] D. H. P. Kang, M. Chen, O. A. Ogunseitan, *Environ. Sci. Technol.* **2013**, *47*, 5495.
[14] S. Randhawa, L. Chopra, *Mater. Today: Proc.* **2022**, *52*, 434.
[15] J. Xu, H. R. Thomas, R. W. Francis, K. R. Lum, J. Wang, B. O. Liang, *J. Power Sources* **2008**, *177*, 512.
[16] J. Dahn, G. M. Ehrlich, in *Linden's Handbook of Batteries*, 5th ed., (Eds: K. W. Beard, T. B. Reddy), McGrawHill, New York **2019**, chap. 17A, pp. 757–824.
[17] Y. H. Chiang, W. Y. Sean, *Reused Lithium-Ion Battery Applied in Water Treatment Plants*, IntechOpen, London, UK **2018**, https://doi.org/10.5772/intechopen.76303.
[18] P. Jagdale, G. Rius, K. Rajan, J. R. Nair, M. Rovere, A. Tagliaferro, C. Gerbaldi, in *Carbon-Based Smart Materials*, (Eds: P. Jagdale,G. Rius, K. Rajan, J. R. Nair, M. Rovere, A. Tagliaferro, C. Gerbaldi), De Gruyter, Berlin **2020**, chap. 6.
[19] J. S. Ribeiro, M. B. J. G. Freitas, J. C. C. Freitas, *J. Environ. Chem. Eng.* **2021**, *9*, 104689.
[20] Z. He, Z. Y. Zhang, F. S. Zhang, *Waste Manage.* **2021**, *124*, 283.
[21] T. K. Ghosh, S. Sadhukhan, D. Rana, A. Bhattacharya, G. Sarkar, D. Chattopadhyay, M. Chakraborty, *Nano-Struct. Nano-Objects* **2020**, *22*, 100454.
[22] P. Ning, Q. Meng, P. Dong, J. Duan, M. Xu, Y. Lin, Y. Zhang, *Waste Manage.* **2020**, *103*, 52.
[23] F. Meng, Q. Liu, R. Kim, J. Wang, G. Liu, A. Ghahreman, *Hydrometallurgy* **2020**, *191*, 105160.
[24] L. P. He, S. Y. Sun, Y. Y. Mu, X. F. Song, J. G. Yu, *ACS Sustainable Chem. Eng.* **2017**, *5*, 714.
[25] L. Li, E. Fan, Y. Guan, X. Zhang, Q. Xue, L. Wei, F. Wu, R. Chen, *ACS Sustainable Chem. Eng.* **2017**, *5*, 5224.
[26] Y. Zheng, W. Song, W. Mo, L. Zhou, J. W. Liu, *RSC Adv.* **2018**, *8*, 8890.
[27] G. P. Nayaka, K. V. Pai, J. Manjanna, S. J. Keny, *Waste Manage.* **2016**, *51*, 234.
[28] L. Li, W. Qu, X. Zhang, J. Lu, R. Chen, F. Wu, K. Amine, *J. Power Sources* **2015**, *282*, 544.
[29] S. Yan, C. Sun, T. Zhou, R. Gao, H. Xie, *Sep. Purif. Technol.* **2021**, *257*, 117930.
[30] E. G. Okonkwo, G. Wheatley, Y. He, *Resour. Conserv. Recycl.* **2021**, *174*, 105813.
[31] P. M. Urias, L. H. Reis Menêzes, V. L. Cardoso, M. M. Resende, J. S. Ferreira, *Environ. Technol.* **2021**, *42*, 4027.
[32] W. Urbańska, M. Osial, *Energies* **2020**, *13*, 6731.
[33] M. Aaltonen, C. Peng, B. P. Wilson, M. Lundström, *Recycling* **2017**, *2*, 20.
[34] X. Chen, C. Guo, H. Ma, J. Li, T. Zhou, L. Cao, D. Kang, *Waste Manage.* **2018**, *75*, 459.
[35] Z.-M. Zhang, S. Chen, Y.-Z. Liang, *Analyst* **2010**, *135*, 1138.
[36] S.-J. Baek, A. Park, Y.-J. Ahna, J. Choo, *Analyst* **2015**, *140*, 250.
[37] H. F. M. Boelens, P. H. C. Eilers, T. Hankemeier, *Anal. Chem.* **2005**, *77*, 7998.
[38] S. He, W. Zhang, L. Liu, Y. Huang, J. He, W. Xie, P. Wu, C. Du, *Anal. Methods* **2014**, *6*, 4402.
[39] K. Grodecki, R. Bozek, W. Strupinski, A. Wysmolek, R. Stepniewski, J. M. Baranowski, *Appl. Phys. Lett.* **2012**, *100*, 261604.
[40] T. M. G. Mohiuddin, A. Lombardo, R. R. Nair, A. Bonetti, G. Savini, R. Jalil, N. Bonini, D. M. Basko, C. Galiotis, N. Marzari, K. S. Novoselov, A. K. Geim, A. C. Ferrari, *Phys. Rev. B* **2009**, *79*, 205433.
[41] L. M. Malard, M. A. Pimenta, G. Dresselhaus, M. S. Dresselhaus, *Phys. Rep.* **2009**, *473*, 51.
[42] J. Jiang, R. Pachter, A. E. Islam, B. Maruyama, J. J. Boeckl, *Chem. Phys. Lett.* **2016**, *663*, 79.
[43] M. A. Azam, M. F. A. Aziz, N. N. Zulkapli, G. Omar, R. F. Munawar, M. S. M. Suan, N. E. Safie, *Diamond Relat. Mater.* **2020**, *104*, 107767.
[44] H. Kato, N. Itagaki, H. J. Im, *Carbon* **2019**, *141*, 76.
[45] S. Krukowski, J. Sołtys, J. Borysiuk, J. Piechota, *J. Cryst. Growth* **2014**, *401*, 869.
[46] N. Sheremetyeva, M. Lamparski, C. Daniels, B. Van Troeye, V. Meunier, *Carbon* **2020**, *169*, 455.
[47] G. S. Papanai, I. Sharma, B. K. Gupta, *Mater. Today Commun.* **2020**, *22*, 100795.
[48] J. J. Morgan, M. F. Craciun, S. J. Eichhorn, *Compos. Sci. Technol.* **2019**, *177*, 34.
[49] D. L. Silva, J. L. E. Campos, T. F. D. Fernandes, J. N. Rocha, L. R. P. Machado, E. M. Soares, D. R. Miquita, H. Miranda, C. Rabelo, O. P. Vilela Neto, A. Jorio, L. G. Cançado, *Carbon* **2020**, *161*, 181.
[50] A. Y. Lee, K. Yang, N. D. Anh, C. Park, S. M. Lee, T. G. Lee, M. S. Jeong, *Appl. Surf. Sci.* **2021**, *536*, 147990.
[51] J. Ribeiro-Soares, M. E. Oliveros, C. Garin, M. V. David, L. G. P. Martins, C. A. Almeida, E. H. Martins Ferreira, K. Takai, T. Enoki, R. Magalhães-Paniago, A. Malachias, A. Jorio, B. S. Archanjo, C. A. Achete, L. G. Cançado, *Carbon* **2015**, *95*, 646.
[52] K. Grodecki, *Mater. Elektron.* **2013**, *41*, 47.
[53] H. Liang, X. Qiu, S. Zhang, Z. He, W. Zhu, L. Chen, *Electrochem. Commun.* **2004**, *6*, 505.
[54] K. S. Kim, Y. J. Park, *Nanoscale Res. Lett.* **2012**, *7*, 47.
[55] Z. Q. Li, C. J. Lu, Z. P. Xia, Z. Luo, *Carbon* **2007**, *45*, 1686.
[56] T. Qiu, J. G. Yang, X. J. Bai, Y. L. Wang, *RSC Adv.* **2019**, *9*, 12737.
[57] R. Quadir, F. Gulshan, *Mater. Sci. Appl.* **2018**, *9*, 142.
[58] W. S. Chen, H. J. Ho, *Metals* **2018**, *8*, 321.

© 2022 Wiley-VCH GmbH